Impact on short-lived climate forcers (SLCFs) from a realistic land-use change scenario via changes in biogenic emissions

C. E. Scott[1]*, S. A. Monks[2,3], D. V. Spracklen[1], S. R. Arnold[1], P. M. Forster[1], A. Rap[1]
K. S. Carslaw[1], M. P. Chipperfield[1], C. L. S. Reddington[1], C. Wilson[1]

[1]Institute for Climate and Atmospheric Science, School of Earth and Environment, University of Leeds, Leeds, UK
[2]Cooperative Institute for Research in Environmental Sciences, University of Colorado, Boulder, Colorado, USA
[3]Chemical Sciences Division, NOAA Earth System Research Laboratory, Boulder, Colorado, USA
*Corresponding author: c.e.scott@leeds.ac.uk

Abstract

More than one quarter of natural forests have been cleared by humans to make way for other land-uses, with changes to forest cover projected to continue. The climate impact of land-use change (LUC) is dependent upon the relative strength of several biogeophysical and biogeochemical effects[1-4]. In addition to affecting the surface albedo and exchanging carbon dioxide (CO_2) and moisture with the atmosphere, vegetation emits biogenic volatile organic compounds (BVOCs), altering the formation of short-lived climate forcers (SLCFs) including aerosol, ozone (O_3) and methane (CH_4).

Once emitted, BVOCs are rapidly oxidised by O_3, and the hydroxyl (OH) and nitrate (NO_3) radicals. These oxidation reactions yield secondary organic products which are implicated in the formation and growth of aerosol particles and are estimated to have a negative radiative effect on the climate (i.e. a cooling). These reactions also deplete OH, increasing the atmospheric lifetime of CH_4, and directly affect concentrations of O_3; the latter two being greenhouse gases which impose a positive radiative effect (i.e. a warming) on the climate.

Our previous work[5] assessing idealised deforestation scenarios, found a positive radiative effect due to changes in SLCFs; however, since the radiative effects associated with changes to SLCFs result from a combination of non-linear processes it may not be appropriate to scale radiative effects from complete deforestation scenarios according to the deforestation extent. Here we combine a land-surface model, a chemical transport model, a global aerosol model, and a radiative transfer model to assess the net radiative effect of changes in SLCFs due to historical LUC between the years 1850 and 2000.

We find that LUC between 1850 and 2000 has reduced both BVOC emission and subsequent SOA formation by 13%. The positive aerosol radiative effects associated with a reduction in biogenic SOA (0.02 W m^{-2} and 0.008 W m^{-2} for the DRE and AIE respectively) outweigh the negative radiative effects due to a reduction in O_3 and CH_4 (-0.02 W m^{-2} and -0.007 W m^{-2} respectively), resulting in a small net SLCF RE of 0.004 W m^{-2}.

Introduction

Land-use change (LUC) has accompanied population growth for several thousand years, and particularly the past 300 years[6]. Prior to 1850, deforestation occurred predominantly in the temperate regions of Europe, Asia and North America; from around 1900 onwards, the majority of deforestation has occurred in tropical regions, specifically South and Central America, South-east Asia and Central Africa[7]. Whilst tropical deforestation continues to drive high rates of forest loss globally (a total of 2.3 million km^2 between 2000 and 2012), afforestation and natural forest regrowth due to agricultural abandonment have led to gains in forest cover (0.8 million km^2 between 2000 and 2012)[8]. Projections of future LUC vary widely in terms of spatial extent and timing[9], and a thorough understanding of the climatic impacts of LUC is needed to inform climate mitigation policies[10].

The impact of LUC on climate is determined by several biogeophysical and biogeochemical interactions between vegetation and the atmosphere[1-4]. The process of converting vegetated land from one type to another can alter the surface albedo and modify evapotranspiration (biogeophysical interactions), as well as resulting in the emission of carbon dioxide (CO_2; a biogeochemical interaction). Forests are darker in colour than crop or pastureland so conversion of forests to agricultural land tends to increases surface albedo, exerting a negative radiative effect on the climate[3]. Emission of CO_2 from LUC, either through forest burning or removal and decay of wood products, increases the concentration of CO_2 in the atmosphere[11], exerting a warming effect on the climate.

In addition to these effects, forests and vegetation have an influence on the composition of the atmosphere through the emission of biogenic volatile organic compounds (BVOCs). If LUC alters the emission of BVOCs, it may affect the climate by changing the concentrations of short-lived climate forcers (SLCFs) including ozone (O_3), methane (CH_4) and aerosols; an additional biogeochemical interaction. BVOCs are rapidly oxidised by the hydroxyl radical (OH), the nitrate radical (NO_3) and O_3, affecting the oxidative capacity of the atmosphere and therefore concentrations of the greenhouse gases O_3 and CH_4. In the presence of nitrogen oxides (NO_x), BVOCs also contribute to the production of O_3 in the troposphere, complicating their impact on climate[12].

The oxidation of BVOCs generates products with low enough volatility to enter the particle phase, as secondary organic aerosol (SOA). These oxidation products may participate in the formation of new particles[13-15] and condense onto existing particles in the atmosphere, aiding their growth to larger sizes[16-18]. These particles can interact directly with incoming solar radiation (a direct radiative effect or forcing) and also modify the microphysical properties of clouds (an indirect radiative effect or forcing). Biogenic SOA very likely exerts a negative radiative effect on the climate, via both the direct and first aerosol indirect (i.e., cloud albedo) effects[19, 20].

Assessments of the overall impact of LUC have traditionally considered the balance between carbon cycling and alterations to surface fluxes of energy and water[2, 4, 21, 22]. Recently, studies have begun to quantify the impacts of deforestation and LUC associated with changes to the concentration of SLCFs[5, 23-26].

In an integrated study of the impacts of historical LUC on SLCFs, Unger[23] found that the reduction in BVOC emissions due to LUC since 1850 may have caused an overall climate cooling due to reductions in O_3 and CH_4 concentrations, outweighing the (direct radiative) impact of decreased biogenic SOA formation. Using the same historical land-use trajectory[27], but a different land surface model, Heald and Geddes[26] diagnosed a much smaller cooling associated with O_3 reduction (than ref[23]), but a much stronger cooling effect due to increased ammonia emission from agriculture and subsequent nitrate aerosol formation. Conversely, Ward et al.[25], simulate a LUC related increase in O_3 concentration over the historical period, and therefore warming effect, attributed to changes in fire related emissions. This range of published values highlights the complexity associated with diagnosing radiative impacts from any amount of LUC.

Here, we explore the effect of historical LUC (1850 - 2000) on BVOC emissions, and the radiative impacts of subsequent changes to SLCFs. To do this we evaluate O_3, CH_4 and aerosol concentrations in the year 2000 using either year 2000 land-cover (experiment 2000_2000LC) or 1850 land-cover (experiment 2000_1850LC). Our focus is on the impact of changes in BVOC emissions and so we do not include trace gas emissions associated with subsequent agricultural activities. Our study builds on previous analyses of the impacts of historical LUC via changes in BVOC emissions[23] by also considering the strength of the aerosol indirect effect which may enhance the positive direct radiative effect due to decreased SOA production.

Experimental

To estimate the radiative impacts of land-use change we combine a land-surface model with a chemical transport model, global aerosol model, and radiative transfer model. The land surface model is used to estimate the changes in BVOC emissions that have occurred due to LUC. We use a global chemical transport model including a detailed description of aerosol microphysics to calculate the impacts of altered BVOC emissions on atmospheric chemistry and aerosol. We then use the radiative transfer model to calculate the radiative impacts of the altered chemistry and aerosol. In this work we focus on the impact that historical LUC has had in the present day atmosphere.

Land surface model

We use the Community Land Model (CLMv4.5; ref[28, 29]), coupled to the Model of Emissions of Gases and Aerosols from Nature (MEGANv2.1; ref[30]), to quantify the effects of LUC on the emission of BVOCs.

The CLM operates at a horizontal resolution of 0.9° x 1.25° and here we use the offline configuration, i.e., not coupled to either the Community Atmosphere Model (CAM) or the Community Earth System Model (CESM),

with atmospheric forcing (precipitation, solar radiation, atmospheric pressure, specific humidity, temperature and wind) taken from an observationally derived dataset (CRUNCEP[31]) which is a combination of CRU TS3.2 monthly data (covering 1901 – 2002; ref[32]) and hourly NCEP reanalysis data (covering 1948-2010; ref[33]). Between 1850 and 1900, prior to the start of the CRUNCEP dataset, atmospheric forcing data 1901-1920 from the CRUNCEP dataset is repeatedly cycled.

The surface of each grid cell in the CLM is divided into 15 different plant functional types (PFTs), plus non-vegetated surface. A harmonised land-use dataset, derived from a global land model (GLM)[27, 34] and based on the historical crop and pasture maps of the History Database of the Global Environment (HYDE 3.1)[6, 35], has been adapted specifically for the CLM[36] and remains consistent with MODIS data[37,38] for the year 2000. Figure 1 illustrates the area covered by groupings of the major PFTs from this dataset during the period 1850 – 2000.

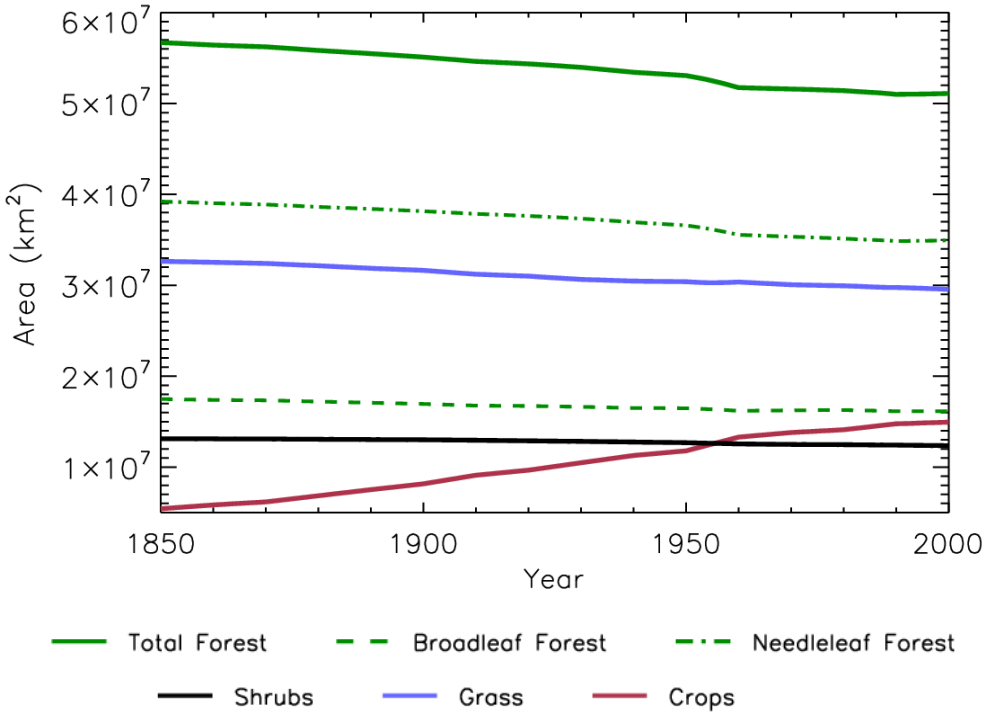

Figure 1: Total area occupied by combined PFTs, as represented in the CLM, during the years 1850 - 2000.

We perform two simulations with the CLM, covering the years 1850 to 2000. In the first simulation, land-cover evolves over time according to the 1850-2000 historical land-cover dataset; climate and carbon dioxide (CO_2) concentrations also vary with time (used to obtain emissions for the 2000_2000LC experiment). In the second simulation, whilst climate and CO_2 concentration vary with time, land-cover is held fixed with the 1850 distribution of PFTs (used to obtain emissions for the 2000_1850LC experiment). Holding land-cover fixed but allowing climate and CO_2 to vary means that the leaf area index (LAI) for vegetated surfaces reflects the climatic conditions in any given year of the simulation.

Within the CLM, emissions of BVOCs are calculated using the MEGANv2.1 (ref[30]) algorithm, according to the PFT distribution and climatic conditions. In the simulation in which land-cover varies over time, we simulate a global total monoterpene (sum of individual monoterpenes) emission of 142 Tg(C) a^{-1} and total isoprene emission of 400 Tg(C) a^{-1} for the year 2000, values which lie within the very broad range of previous emission estimates (30-156 Tg(C) a^{-1} for monoterpenes and 309-706 Tg(C) a^{-1} for isoprene[30, 39-41]).

Chemical transport model and aerosol microphysics model

To diagnose LUC induced changes to gas-phase and aerosol species we use the TOMCAT chemical transport model[42] and the GLObal Model of Aerosol Processes (GLOMAP)[43, 44]. All simulations are performed for the year 2000, with one year spin-up. We use a horizontal resolution of 2.8° × 2.8° and 31 pressure levels from the surface to 10 hPa; meteorology in both TOMCAT and GLOMAP is driven by European Centre for Medium-Range Weather Forecasts (ECMWF; ERA-Interim) reanalyses at 6-hourly intervals, and cloud fields are taken from the International Satellite Cloud Climatology Project (ISCCP) archive[45], both for the year 2000.

We use the modal version of GLOMAP to simulate the number, size and distribution of particles in the atmosphere. GLOMAP-mode carries information about particle composition and number in five log-normal size modes, including soluble nucleation, Aitken, accumulation and coarse modes, as well as an insoluble Aitken mode. GLOMAP includes representations of new particle formation, particle growth (via coagulation, condensation and cloud processing), wet deposition, dry deposition, and, in- and below-cloud scavenging. Material in the particle phase is classified into four components: sea-salt, sulphate, black carbon (BC) and particulate organic matter (POM; containing both primary and secondary organic species).

In GLOMAP, anthropogenic emissions (BC, POM and sulphur dioxide; SO_2) from fossil and biofuel combustion are taken from refs[46,47], with monthly varying biomass burning emissions (BC, POM and SO_2) from the Global Fire Emissions Database (GFEDv3; ref[48]) for the year 2000. GLOMAP also includes SO_2 emissions from both continuous[49] and explosive[50] volcanic eruptions, and calculates emissions of dimethyl-sulphide (DMS) from phytoplankton.

Gas-phase secondary organic products are generated from the oxidation of monoterpenes and isoprene by O_3, OH and NO_3, with rate constants and molar yields (13% for monoterpenes and 3% for isoprene) from ref[20]. The products of monoterpene and isoprene oxidation are tracked independently and are assumed to be non-volatile, condensing irreversibly onto existing particles according to their Fuchs-Sutugin-corrected surface area[51]; in previous work we explored the sensitivity of aerosol radiative effects to this approach to partitioning[52].

The new particle formation rate is assumed to be dependent upon the concentration of both sulphuric acid and the secondary organic product from monoterpene oxidation[13]. The new particle formation rate (J*) is parameterised according to Eqn. 1 with $k = 5 \times 10^{-13}$ s^{-1}; only the secondary organic product from monoterpene oxidation may

participate as the nucleating organic (NucOrg) in this process, the product of isoprene oxidation contributes only to condensational growth. J* represents the formation of particles at 1.5 nm, with their growth to 3 nm parameterised according to ref[53] and described in ref[20, 52].

$$J^{*}_{ORG} = k\,[H_2SO_4][\,NucOrg] \quad (1)$$

GLOMAP uses 6-hourly monthly-mean oxidant concentrations (O_3, OH, NO_3, HO_2 and H_2O_2), from equivalent LUC simulations performed with the TOMCAT chemical transport model; this simplification means that changes to aerosol processes due to LUC do not feedback onto tropospheric chemistry. In GLOMAP O_3, OH and NO_3 take part in the oxidation of BVOCs and formation of SOA, whereas HO_2 and H_2O_2 concentrations are used in the in-cloud oxidation of SO_2, described in ref.[43]; H_2O_2 is treated semi-prognostically, being replenished by HO_2 self-reaction.

We use the TOMCAT chemical transport model, described in detail in ref[54, 55], to simulate the impact of LUC on tropospheric chemistry. The model includes extended VOC degradation chemistry (ExTC) which simulates the oxidation of several C_2 to C_7 hydrocarbons. Isoprene oxidation follows the Mainz Isoprene Mechanism[56], and monoterpene oxidation is based on the MOZART-3 scheme[57, 58]. Gas-phase emissions are those prepared for the POLARCAT Model Intercomparison Project (POLMIP)[59], taken from the Streets v1.2 anthropogenic emissions inventory[60] and the GFEDv3.1biomass burning emission inventory[48]. In addition to the BVOCs calculated offline by MEGAN, natural ocean and soil emissions are included from the POET emission inventory[61] and lightning emissions are calculated online. NO_x emissions total 143.5 Tg(NO_x) yr^{-1}. The tropospheric burden of O_3 is 290 Tg (in our year 2000 simulation that includes present-day LUC). Methane (CH_4) emissions include GFEDv3.1 fire[48], EDGARv3.2 anthropogenic[62], wetland and rice[63], and other natural emissions (treated as in refs.[64, 65]), totalling 544.9 Tg(CH_4) yr^{-1}. These are emitted into the boundary layer of the model and the surface concentrations are scaled at every time step to match a global mean concentration of 1800 ppbv, allowing a realistic spatial distribution, consistent with high and low emission regions. A diurnal cycle in the BVOC isoprene emissions is imposed online in the model to reflect the variability in isoprene emission with daylight. Loss of N_2O_5 by aerosol uptake is calculated using size-resolved aerosol from the GLOMAP model[43]; these do not vary between the different LUC scenarios.

Since the nature of the land-surface affects the dry deposition of both gases and aerosol, the characteristics of the model land-surface are modified to reflect the simulated pattern of LUC. In GLOMAP, roughness lengths and characteristic radii for different land surface types are taken from ref.[66]. In TOMCAT, the land type classification map used to calculate the dry deposition of relevant gas phase-species is altered to reflect the distribution of land-cover types for the relevant year.

Calculation of radiative effects

We calculate the radiative impact of LUC-induced changes to the concentration of SLCFs using the Suite Of Community RAdiative Transfer codes based on Edwards and Slingo[67] (SOCRATES) with nine bands in the longwave (LW) and six bands in the shortwave (SW). We use an offline configuration with a monthly mean climatology (temperature and water vapour concentrations) based on ECMWF reanalysis data, with cloud fields from the ISCCP-D2 archive[45] for the year 2000 (described in ref.[19]). To isolate the impact of changes to SLCFs, surface albedo is held fixed at year 2000 conditions. The sensitivity of direct and indirect aerosol radiative effects to the cloud climatology used (i.e. single year v. multi-annual mean) has previously been shown to be small[19].

Aerosol radiative effects

Aerosol radiative effects are calculated by considering the difference in net (SW + LW) top-of-atmosphere all-sky radiative flux between each experiment. The direct radiative effect (DRE) for each experiment is obtained using the aerosol optical properties (scattering and absorption coefficients and the asymmetry parameter), computed for each size mode and spectral band[68]. The aerosol first indirect effect (AIE), or cloud albedo effect, is determined from the radiative perturbation induced by the change to cloud droplet number concentration (CDNC) associated with LUC. This approach has been described in previous studies[19, 20, 69].

Cloud droplet number concentrations are calculated[70-72] from the monthly mean aerosol size distribution, assuming a uniform updraught velocity of 0.15 m s^{-1} over sea and 0.3 m s^{-1} over land. The critical supersaturation is calculated using the hygroscopicity parameter (κ) approach[73]. A multi-component κ is obtained by weighting individual κ values by the volume fraction of each component. We assign the following individual κ values: sulphate (0.61, assuming ammonium sulphate), sea-salt (1.28), black carbon (0.0), and particulate organic matter (0.1); there is substantial uncertainty associated with the hygroscopicity of organic material observed in the atmosphere, but κ values close to 0.1 have been reported for organic aerosol produced from the oxidation of BVOCs[74-77].

To calculate the first AIE, a uniform control cloud droplet effective radius (r_{e1}) of 10 μm is assumed to maintain consistency with the ISCCP derivation of the liquid water path, and for each deforestation experiment the effective radius (r_{e2}) is calculated as in Eqn. 2, from monthly mean cloud droplet number fields $CDNC_1$ and $CDNC_2$ respectively (where $CDNC_1$ represents the control simulation (2000_2000LC), and $CDNC_2$ represents the scenario in which LUC has not occurred (2000_1850LC)).

$$r_{e_2} = r_{e_1} \times \left[\frac{CDNC_1}{CDNC_2}\right]^{\frac{1}{3}} \quad (2)$$

The first AIE associated with LUC is then calculated by comparing net radiative fluxes using the varying r_{e2} values derived for the above perturbation experiment, to those of a control simulation with fixed r_{e1}. In these offline experiments, we do not calculate the second aerosol indirect (cloud lifetime) effect.

O_3 and CH_4 radiative effects

The radiative forcing associated with changes to tropospheric O_3 concentrations are calculated using the radiative kernels developed by ref.[78]. It has been shown that O_3 radiative effects calculated using the kernel approach are in very good agreement to radiative effects calculated using the SOCRATES radiative transfer model, both for O_3 concentrations from the TOMCAT model and those calculated using O_3 retrieved from Tropospheric Emission Spectrometer (TES) satellite measurements[78].

Changes to O_3 concentration also induce a change in the concentration of the hydroxyl radical (OH), and therefore CH_4 which in turn affects peroxy radical production and has an impact on O_3. We calculate a change in O_3 concentration in response to this "primary mode" of tropospheric photochemistry following ref.[79] and diagnose an appropriate radiative effect using a value of 0.032 W m^{-2} DU^{-1} (following ref.[25, 80]). We add this primary mode response to the RE diagnosed directly from O_3 changes using the radiative kernel.

As the lifetime of CH_4 is approximately 10 years, our one-year TOMCAT simulations cannot be used to determine the effect of the changing source of BVOCs on CH_4 concentrations. Therefore, to determine the radiative effect due to a change in CH_4 concentration, the change in global annual mean (CH_4 reaction weighted, using a climatological tropopause)[81] concentration of OH in the troposphere is used to estimate the change in the tropospheric chemical CH_4 lifetime, and hence the change in steady-state CH_4 concentration[82, 83], assuming a feedback factor of 1.34 (ref.[84]). The change in steady-state CH_4 concentration is used to quantify the global annual mean radiative effect[85], assuming a present-day N_2O concentration of 324.2 ppb (ref.[86]).

Results & Discussion

Historical land-use change

Table 1 provides the global total area represented by groupings of the 15 PFTs represented in the CLM. Land-use change between 1850 and 2000 is characterised by global forest loss (a reduction of approx. 5.6 million km^2) and an expansion of cropland (an increase of approx. 9.5 million km^2).

Figure 2 illustrates the spatial distribution of LUC between 1850 and 2000. Both temperate and tropical regions experience predominantly forest loss, but west Europe and the eastern coast of North America see expansion of both broadleaf and needleleaf forest due to agricultural abandonment and reforestation.

Table 1: Area occupied by vegetated land classes in 1850 and 2000 (refs[6, 27, 36]).

Plant functional type (PFT)	**Area occupied by PFT (10^6 km^2)**		
	1850	**2000**	**Change from 1850 to 2000**
Broadleaf forest (combined total of tropical evergreen / temperate evergreen / tropical deciduous / temperate deciduous / boreal deciduous forest)	39.2	35.0	-4.3 (-10.9%)
Needleleaf forest (combined total temperate evergreen / boreal evergreen / boreal deciduous forest)	17.5	16.2	-1.3 (-7.6%)
Total forest (combined total of broadleaf and needleleaf forest)	56.7	51.1	-5.6 (-9.9 %)
Total grass (combined total of C_3 Arctic grass / C_3 grass / C_4 grass)	32.6	29.5	-3.1 (-9.5%)
Total crop	5.4	14.9	+9.5 (+175.6%)

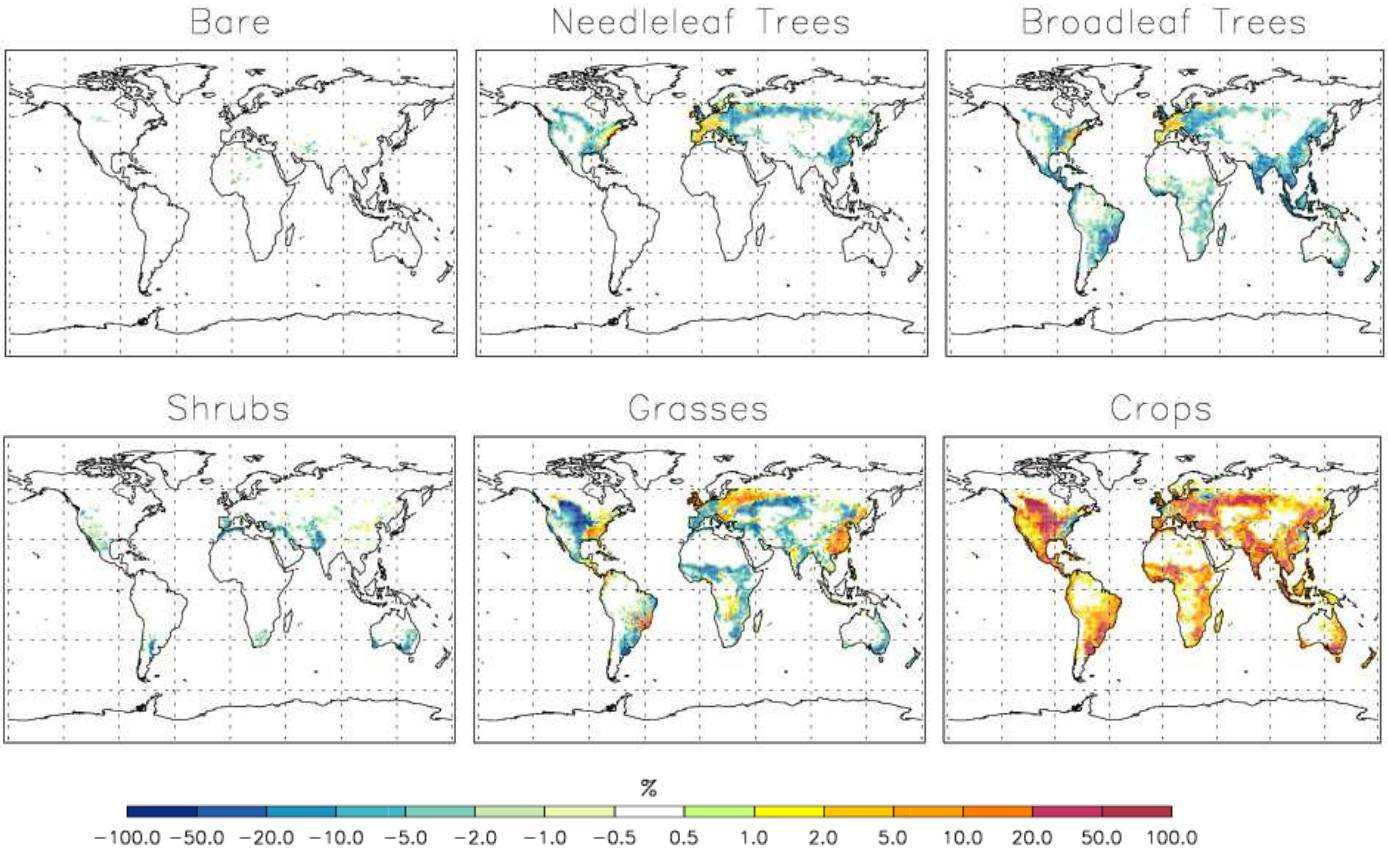

Figure 2: Percentage change to combined categories of plant functional types (refs[6, 27, 36]) between the year 1850 and the year 2000 (blue colours indicate a reduced area in 2000 as compared to 1850).

Impact of land-use change on biogenic emissions

Globally, LUC between 1850 and 2000 has reduced isoprene and monoterpene emissions both by 13%, with a subsequent reduction in SOA production from 42 Tg(SOA) a^{-1} to 37 Tg(SOA) a^{-1}. The amount of SOA produced in the present-day atmosphere is poorly constrained, with estimates[87-93] ranging between 12 and 1870 Tg(SOA) a^{-1}. The reduction in BVOC emission and SOA production simulated due to LUC occurs as a result of the much lower BVOC emission factors assigned to cropland as compared to either grass or forested land[30].

Table 2: BVOC emission and SOA production totals for each simulation.

	Global annual total					
	Isoprene emission (Tg(C) a^{-1}) **and % change due to LUC**		**Total monoterpene emission** (Tg(C) a^{-1}) **and % change due to LUC**		**SOA generated** (Tg(SOA) a^{-1}) **and % change due to LUC**	
2000_1850LC (year 2000 climate and CO_2 concentration; land-use configuration from 1850)	460		164		42	
2000_2000LC	400	-13%	142	-13%	37	-13%

(year 2000 climate and CO_2 concentration; land-use configuration from 2000)						

Aerosol radiative effects due to land-use change

Globally, LUC since 1850 has had a positive direct radiative effect (DRE) of 0.025 W m^{-2} due to reduced production of biogenic SOA. This positive RE occurs because fewer particles grow large enough to interact directly with radiation in the atmosphere. Figure 3 (left) shows the spatial distribution of the DRE which coincides with the regions of greatest forest loss (Figure 2). The largest DRE occurs over tropical regions, exceeding 0.5 W m^{-2} over parts of Southeast Asia and South America. The DRE we simulate is comparable in magnitude to that calculated by Heald and Geddes[26] (0.017 W m^{-2}), but smaller than that calculated by Unger[23] (0.09 W m^{-2}); this reflects the greater reduction in BVOC emissions (-35%), and therefore SOA production, due to land-use change simulated by Unger.

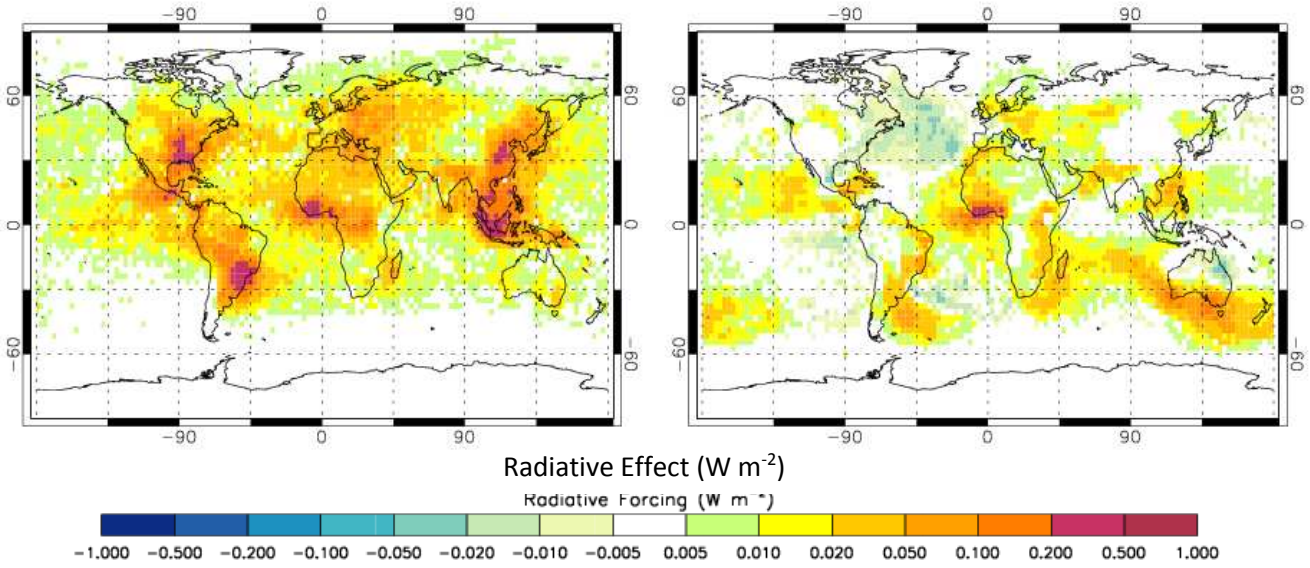

Figure 3: Annual mean direct radiative effect (left) and first aerosol indirect radiative effect (right) in the year 2000, due to LUC since 1850.

Globally, LUC since 1850 has had a small positive first aerosol indirect effect (AIE; or cloud albedo effect) of 0.008 W m^{-2} due to an overall reduction in the number of particles able to form cloud droplets. Figure 4 illustrates the spatial distribution of the change to cloud droplet number concentration (CDNC) that leads to the AIE shown in Figure 3 (right). Reductions in CDNC are greatest (up to 40%) over the regions of forest loss, but the simulated AIE is greatest in regions where a reduction in CDNC coincides with high cloud fraction and low background CDNC (i.e. regions with high percentage decreases in Figure 4 (right)).

A small increase in CDNC over the North Atlantic ocean (< +0.5%; Figure 4 (right)) leads to a small negative regional AIE (< -0.05 W m^{-2}; Figure 3 (right)). As described previously[20], changes to the source of condensable material in the atmosphere (such as sulphuric acid and secondary organic species) can affect particle

concentrations in geographically distant locations by altering the condensation sink and subsequent rate of nucleation in the upper troposphere, or by enhancing the aging rate of non-hydrophilic particles.

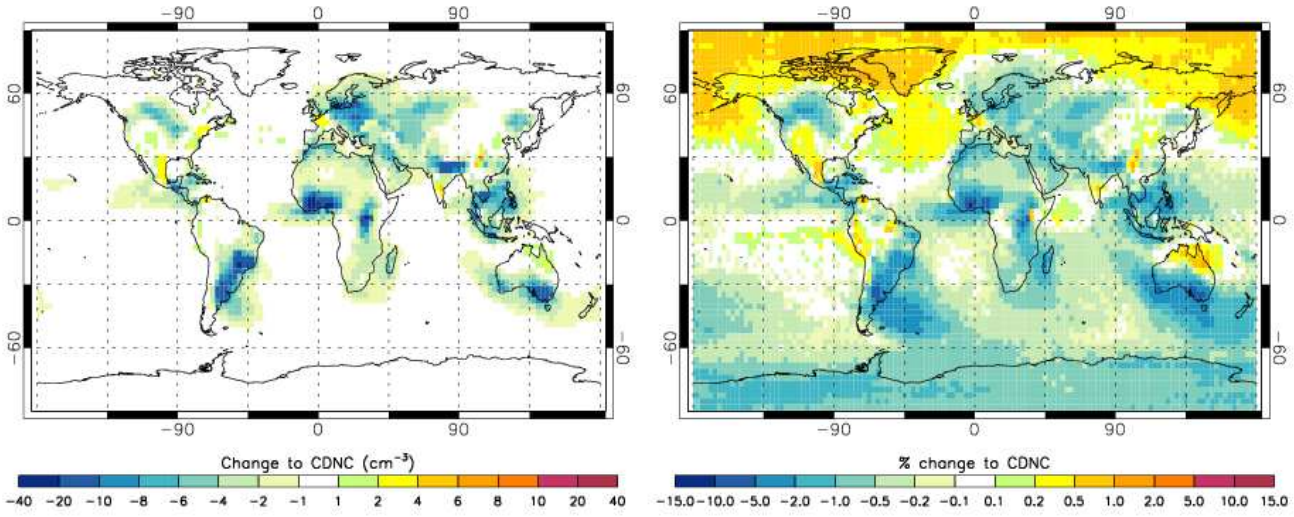

Figure 4: Annual mean change in cloud droplet number concentration (in the model level which corresponds to low level cloud base; mean pressure of approx. 900 hPa) in the year 2000, due to LUC since 1850; absolute change (left) and percentage change (right).

Impact of land-use change on gas-phase species

In most locations, NO_x concentrations are sufficiently high that BVOCs, particularly isoprene, contribute to the production of O_3. The reduction in BVOC emissions associated with LUC therefore leads to a decrease in surface O_3 concentration across much of the planet (Figure 5 (left)). Where modelled NO_x concentrations are lower, direct reaction of BVOCs with O_3 out-competes O_3 production from BVOC oxidation; in these locations, the reduction in BVOC emission associated with LUC leads to an increase in annual mean O_3 concentrations at the surface (up to 4 ppbv). This effect is combined with the decrease in O_3 dry deposition associated with conversion from forests to crop or grassland, enhancing any increases in O_3 concentrations. However, any increases in O_3 concentration diminish with altitude (Figure 5 (right)) and the zonal mean change in O_3 is negative throughout the troposphere at all latitudes (Figure 6).

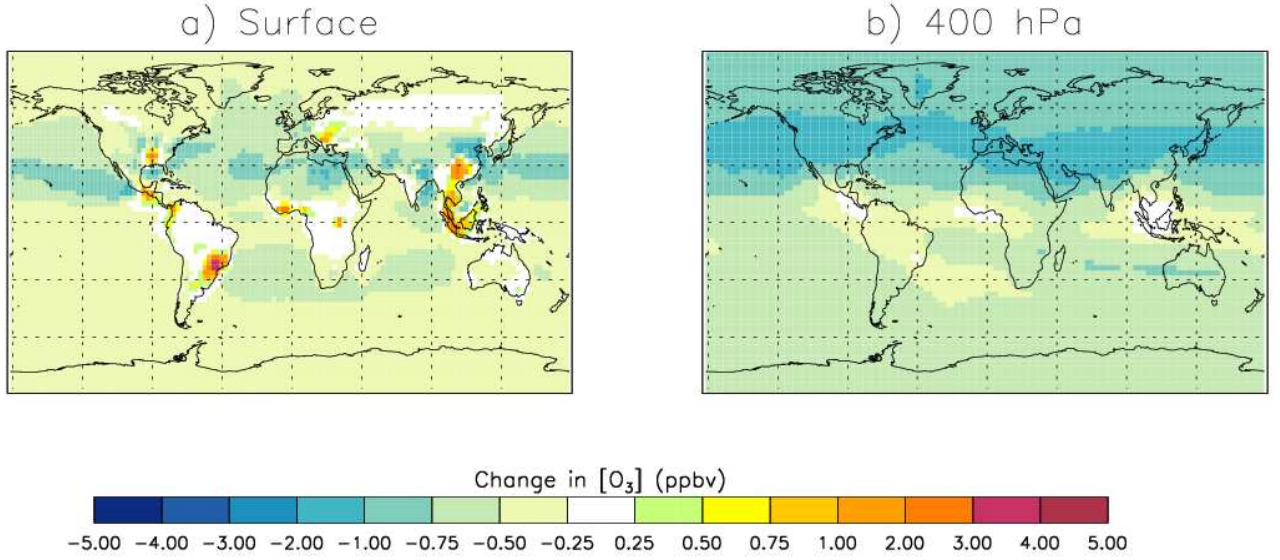

Figure 5: Annual mean change to O_3 concentration (ppbv) in the year 2000 due to LUC since 1850, in TOMCAT model surface layer (left) and at 400 hPa (right).

The reduction in BVOC emissions due to LUC since 1850 has led to a global annual mean tropospheric O_3 radiative effect of -0.02 W m^{-2} (direct O_3 RE plus "primary mode" response). Our simulated O_3 RE due to historical LUC, is lower in magnitude than that diagnosed by Unger[23] (-0.13 W m^{-2}) which may reflect the smaller perturbation to BVOC emissions in our study or differing model sensitivities to perturbations in O_3 precursors.

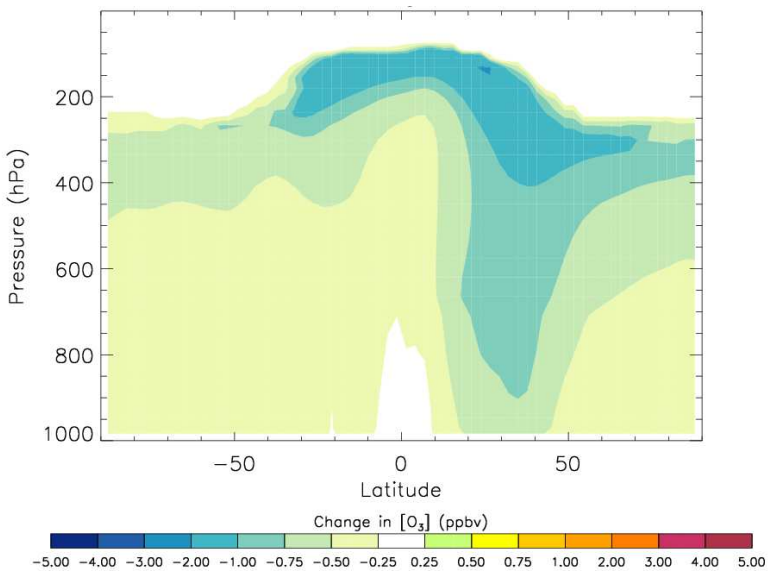

Figure 6: Annual zonal mean change to O_3 concentration (ppbv) in the year 2000 due to LUC since 1850, calculated using the TOMCAT model.

The reduction in BVOC emission associated with global LUC leads to an increase in annual tropospheric mean OH concentration, from 7.51× 10^5 to 7.55 × 10^5 molecules cm^{-3}, which reduces the lifetime of CH_4 from 10.64 years to 10.55 years (within the range of values simulated by the ACCMIP models[94]). This change in CH_4 lifetime is used to diagnose a reduction in steady-state CH_4 concentration of 20 ppb due to global LUC, and an RE of -

0.007 Wm^{-2}. However, uncertainties remain in our understanding of the role of OH during isoprene oxidation[95, 96] which will influence the sensitivity of CH_4 concentrations to changes in BVOC emissions.

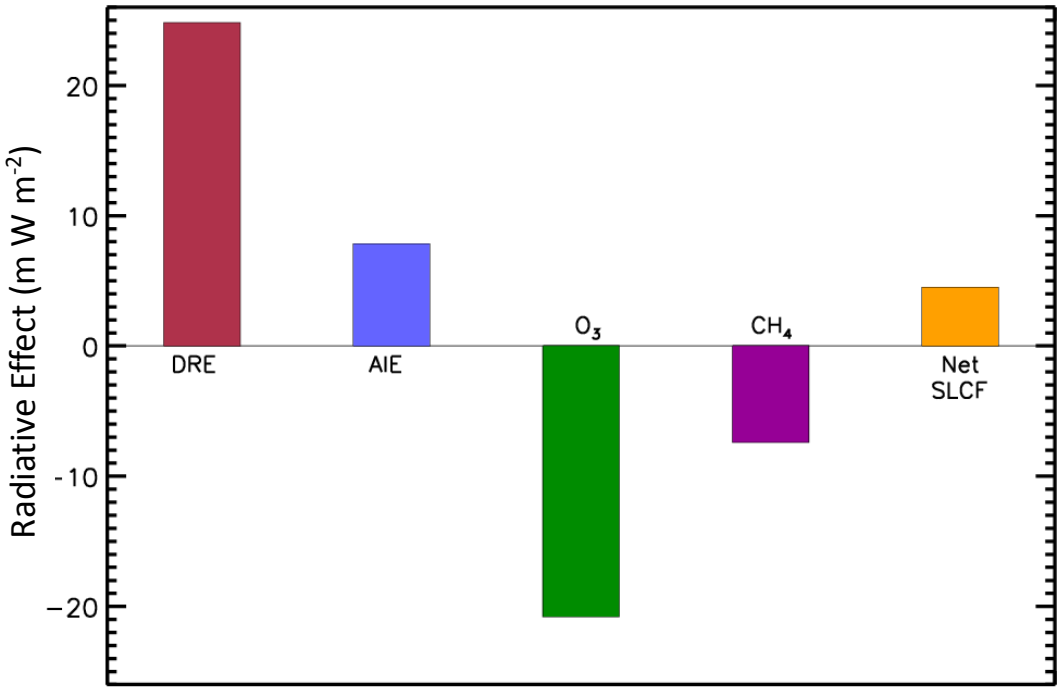

Figure 7: **Global annual mean radiative effects (REs) associated with changes in the concentrations of SLCFs** due to LUC between 1850 and 2000. Bars represent the net RE (orange) and the aerosol direct radiative effect (DRE; in red), first aerosol indirect radiative effect (AIE; in blue) and RE due to changes in O_3 (green) and CH_4 (purple).

We calculate the combined impact of LUC on the concentration of SLCFs through the combination of aerosol (DRE and AIE), O_3 and CH_4 REs (Figure 7). The combined RE from SLCFs is a balance between a warming aerosol RE and a cooling due to reductions in O_3 and CH_4. We estimate that LUC since 1850 has had an overall positive RE of 0.004 W m^{-2} due to changes in these SLCFs.

Our study demonstrates the importance of considering aerosol-cloud effects, which other recent studies have not included[23, 26]; if we do not include the first AIE, our combined SLCF RE is negative (-0.003 W m^{-2}). Previous studies of the impact of LUC on SLCFs did not include the first AIE, and may therefore have attributed too much of a negative RE, or cooling effect, to changes in SLCFs from LUC.

Land-use change can dramatically alter fire activity, with associated changes in emissions of trace gases and aerosol[97], which we do not account for here. We also do not yet consider changes to agricultural emissions that accompany LUC which may be important for nitrate aerosol formation and subsequent radiative impact[26]. Future work needs to explore a representation of the complex relationships between land-use change, agriculture and fire with a coupled earth-system approach.

There remain many uncertainties that affect our ability to estimate the impact of changes to BVOC emission on the concentration of SLCFs, these include: the wide range of estimates of present-day global BVOC emission fluxes[30], the role of other reactive BVOCs (e.g., sesquiterpenes[98, 99]) and the mechanisms of tropospheric oxidation of BVOCs[95, 96]. Uncertainties also remain in our understanding of the interaction of biogenic oxidation products with other atmospheric constituents[100], and their role in SOA formation[101], new particle formation[15, 102], and aerosol microphysical processes[18].

Conclusions

We combined a land-surface model with a chemical transport model, global aerosol model, and radiative transfer model to diagnose the radiative effects associated with perturbations to SLCFs (aerosol, O_3, and CH_4) due to a change in BVOC emissions induced by historical LUC.

We find that LUC between 1850 and 2000 has reduced both BVOC emission and subsequent SOA formation by 13%. The positive aerosol radiative effects associated with a reduction in biogenic SOA (0.02 W m^{-2} and 0.008 W m^{-2} for the DRE and AIE respectively) outweigh the negative radiative effects due to a reduction in O_3 and CH_4 (-0.02 W m^{-2} and -0.007 W m^{-2} respectively), resulting in a small net SLCF RE of 0.004 W m^{-2}.

Whilst we have diagnosed the global mean REs associated with changes to SLCF due to historical LUC, policy discussions around future land-use change will require additional information on the sensitivity of the overall climate impact to the specific location of the land-use change.

Data Availability

The datasets generated, and analysed, during the current study are available from the corresponding author on reasonable request.

References

1. G. B. Bonan, Science, 2008, **320**, 1444-1449.
2. G. Bala, K. Caldeira, M. Wickett, T. J. Phillips, D. B. Lobell, C. Delire and A. Mirin, PNAS, 2007, **104**, 6550-6555.
3. R. A. Betts, Nature, 2000, **408**, 187-190.
4. E. L. Davin and N. de Noblet-Ducoudré, Journal of Climate, 2010, **23**, 97-112.
5. C. E. Scott, S. A. Monks, D. V. Spracklen, S. R. Arnold, P. M. Forster, A. Rap, M. Äijälä, P. Artaxo, K. S. Carslaw, M. P. Chipperfield, M. Ehn, S. Gilardoni, L. Heikkinen, M. Kulmala, T. Petäjä, C. L. S. Reddington, L. V. Rizzo, E. Swietlicki, E. Vignati and C. Wilson, under review, 2017.
6. K. Klein Goldewijk, A. Beusen, G. van Drecht and M. de Vos, Global Ecology and Biogeography, 2011, **20**, 73-86.
7. FAO, State of the World's Forests, United Nations, Rome, 2012.
8. M. C. Hansen, P. V. Potapov, R. Moore, M. Hancher, S. A. Turubanova, A. Tyukavina, D. Thau, S. V. Stehman, S. J. Goetz, T. R. Loveland, A. Kommareddy, A. Egorov, L. Chini, C. O. Justice and J. R. G. Townshend, Science, 2013, **342**, 850-853.
9. P. J. Lawrence, J. J. Feddema, G. B. Bonan, G. A. Meehl, B. C. O'Neill, K. W. Oleson, S. Levis, D. M. Lawrence, E. Kluzek, K. Lindsay and P. E. Thornton, Journal of Climate, 2012, **25**, 3071-3095.
10. R. G. Anderson, J. G. Canadell, J. T. Randerson, R. B. Jackson, B. A. Hungate, D. D. Baldocchi, G. A. Ban-Weiss, G. B. Bonan, K. Caldeira, L. Cao, N. S. Diffenbaugh, K. R. Gurney, L. M. Kueppers, B. E. Law, S. Luyssaert and T. L. O'Halloran, Front. Ecol. Environ., 2011, **9**, 174-182.
11. G. R. van der Werf, D. C. Morton, R. S. DeFries, J. G. J. Olivier, P. S. Kasibhatla, R. B. Jackson, G. J. Collatz and J. T. Randerson, Nature Geosci, 2009, **2**, 737-738.
12. P. S. Monks, A. T. Archibald, A. Colette, O. Cooper, M. Coyle, R. Derwent, D. Fowler, C. Granier, K. S. Law, G. E. Mills, D. S. Stevenson, O. Tarasova, V. Thouret, E. von Schneidemesser, R. Sommariva, O. Wild and M. L. Williams, Atmos. Chem. Phys., 2015, **15**, 8889-8973.
13. A. Metzger, B. Verheggen, J. Dommen, J. Duplissy, A. S. H. Prevot, E. Weingartner, I. Riipinen, M. Kulmala, D. V. Spracklen, K. S. Carslaw and U. Baltensperger, Proceedings of the National Academy of Sciences, 2010, **107**, 6646-6651.
14. F. Riccobono, S. Schobesberger, C. E. Scott, J. Dommen, I. K. Ortega, L. Rondo, J. Almeida, A. Amorim, F. Bianchi, M. Breitenlechner, A. David, A. Downard, E. M. Dunne, J. Duplissy, S. Ehrhart, R. C. Flagan, A. Franchin, A. Hansel, H. Junninen, M. K. Kajos, H. Keskinen, A. Kupc, A. Kürten, A. Kvashin, A. Laaksonen, K. Lehtipalo, V. Makhmutov, S. Mathot, T. Nieminen, A. Onnela, T. Petäjä, A. Praplan, F. D. Santos, S. Schallhart, J. H. Seinfeld, M. Sipilä, D. V. Spracklen, Y. Stozhkov, F. Stratmann, A. Tomé, G. Tsagkogeorgas, P. Vaattovaara, Y. Viisanen, A. Vrtala, P. E. Wagner, E. Weingartner, H. Wex, D. Wimmer, K. S. Carslaw, J. Curtius, N. M. Donahue, J. Kirkby, M. Kulmala, D. R. Worsnop and U. Baltensperger, Science, 2014, **344**, 717-721.
15. J. Kirkby, J. Duplissy, K. Sengupta, C. Frege, H. Gordon, C. Williamson, M. Heinritzi, M. Simon, C. Yan, J. Almeida, J. Tröstl, T. Nieminen, I. K. Ortega, R. Wagner, A. Adamov, A. Amorim, A.-K. Bernhammer, F. Bianchi, M. Breitenlechner, S. Brilke, X. Chen, J. Craven, A. Dias, S. Ehrhart, R. C. Flagan, A. Franchin, C. Fuchs, R. Guida, J. Hakala, C. R. Hoyle, T. Jokinen, H. Junninen, J. Kangasluoma, J. Kim, M. Krapf, A. Kürten, A. Laaksonen, K. Lehtipalo, V. Makhmutov, S. Mathot, U. Molteni, A. Onnela, O. Peräkylä, F. Piel, T. Petäjä, A. P. Praplan, K. Pringle, A. Rap, N. A. D. Richards, I. Riipinen, M. P. Rissanen, L. Rondo, N. Sarnela, S. Schobesberger, C. E. Scott, J. H. Seinfeld, M. Sipilä, G. Steiner, Y. Stozhkov, F. Stratmann, A. Tomé, A. Virtanen, A. L. Vogel, A. C. Wagner, P. E. Wagner, E. Weingartner, D. Wimmer, P. M. Winkler, P. Ye, X. Zhang, A. Hansel, J. Dommen, N. M. Donahue, D. R. Worsnop, U. Baltensperger, M. Kulmala, K. S. Carslaw and J. Curtius, Nature, 2016, **533**, 521-526.
16. I. Riipinen, J. R. Pierce, T. Yli-Juuti, T. Nieminen, S. Häkkinen, M. Ehn, H. Junninen, K. Lehtipalo, T. Petäjä, J. Slowik, R. Chang, N. C. Shantz, J. Abbatt, W. R. Leaitch, V. M. Kerminen, D. R. Worsnop, S. N. Pandis, N. M. Donahue and M. Kulmala, Atmos. Chem. Phys., 2011, **11**, 3865-3878.
17. J. R. Pierce, W. R. Leaitch, J. Liggio, D. M. Westervelt, C. D. Wainwright, J. P. D. Abbatt, L. Ahlm, W. Al-Basheer, D. J. Cziczo, K. L. Hayden, A. K. Y. Lee, S. M. Li, L. M. Russell, S. J. Sjostedt, K. B. Strawbridge, M. Travis, A. Vlasenko, J. J. B. Wentzell, H. A. Wiebe, J. P. S. Wong and A. M. Macdonald, Atmos. Chem. Phys., 2012, **12**, 3147-3163.

18. J. Tröstl, W. K. Chuang, H. Gordon, M. Heinritzi, C. Yan, U. Molteni, L. Ahlm, C. Frege, F. Bianchi, R. Wagner, M. Simon, K. Lehtipalo, C. Williamson, J. S. Craven, J. Duplissy, A. Adamov, J. Almeida, A.-K. Bernhammer, M. Breitenlechner, S. Brilke, A. Dias, S. Ehrhart, R. C. Flagan, A. Franchin, C. Fuchs, R. Guida, M. Gysel, A. Hansel, C. R. Hoyle, T. Jokinen, H. Junninen, J. Kangasluoma, H. Keskinen, J. Kim, M. Krapf, A. Kürten, A. Laaksonen, M. Lawler, M. Leiminger, S. Mathot, O. Möhler, T. Nieminen, A. Onnela, T. Petäjä, F. M. Piel, P. Miettinen, M. P. Rissanen, L. Rondo, N. Sarnela, S. Schobesberger, K. Sengupta, M. Sipilä, J. N. Smith, G. Steiner, A. Tomè, A. Virtanen, A. C. Wagner, E. Weingartner, D. Wimmer, P. M. Winkler, P. Ye, K. S. Carslaw, J. Curtius, J. Dommen, J. Kirkby, M. Kulmala, I. Riipinen, D. R. Worsnop, N. M. Donahue and U. Baltensperger, Nature, 2016, **533**, 527-531.
19. A. Rap, C. E. Scott, D. V. Spracklen, N. Bellouin, P. M. Forster, K. S. Carslaw, A. Schmidt and G. Mann, Geophysical Research Letters, 2013, **40**, 3297–3301.
20. C. E. Scott, A. Rap, D. V. Spracklen, P. M. Forster, K. S. Carslaw, G. W. Mann, K. J. Pringle, N. Kivekäs, M. Kulmala, H. Lihavainen and P. Tunved, Atmos. Chem. Phys., 2014, **14**, 447-470.
21. V. K. Arora and A. Montenegro, Nature Geoscience, 2011, **4**, 514-518.
22. R. Alkama and A. Cescatti, Science, 2016, **351**, 600-604.
23. N. Unger, Nature Clim. Change, 2014, **4**, 907-910.
24. S. D. D'Andrea, J. C. Acosta Navarro, S. C. Farina, C. E. Scott, A. Rap, D. K. Farmer, D. V. Spracklen, I. Riipinen and J. R. Pierce, Atmos. Chem. Phys., 2015, **15**, 2247-2268.
25. D. S. Ward, N. M. Mahowald and S. Kloster, Atmos. Chem. Phys., 2014, **14**, 12701-12724.
26. C. L. Heald and J. A. Geddes, Atmos. Chem. Phys., 2016, **16**, 14997-15010.
27. G. C. Hurtt, L. P. Chini, S. Frolking, R. A. Betts, J. Feddema, G. Fischer, J. P. Fisk, K. Hibbard, R. A. Houghton, A. Janetos, C. D. Jones, G. Kindermann, T. Kinoshita, K. Klein Goldewijk, K. Riahi, E. Shevliakova, S. Smith, E. Stehfest, A. Thomson, P. Thornton, D. P. van Vuuren and Y. P. Wang, Clim. Change, 2011, **109**, 117.
28. K. W. Oleson, D. M. Lawrence, G. B. Bonan, B. Drewniak, M. Huang, C. D. Koven, S. Levis, F. Li, W. J. Riley, Z. M. Subin, S.C. Swenson, P. E. Thornton, A. Bozbiyik, R. Fisher, C. L. Heald, E. Kluzek, J.-F. Lamarque, P. J. Lawrence, L. R. Leung, W. Lipscomb, S. Muszala, D. M. Ricciuto, W. Sacks, Y. Sun, J. Tang and Z.-L. Yang, Technical Description of version 4.5 of the Community Land Model (CLM), National Centre for Atmospheric Research, Boulder, Colorado, 2013.
29. D. M. Lawrence, K. W. Oleson, M. G. Flanner, P. E. Thornton, S. C. Swenson, P. J. Lawrence, X. Zeng, Z.-L. Yang, S. Levis, K. Sakaguchi, G. B. Bonan and A. G. Slater, Journal of Advances in Modeling Earth Systems, 2011, **3**, M03001.
30. A. B. Guenther, X. Jiang, C. L. Heald, T. Sakulyanontvittaya, T. Duhl, L. K. Emmons and X. Wang, Geosci. Model Dev., 2012, **5**, 1471-1492.
31. N. Viovy, Journal, 2011.
32. T. D. Mitchell and P. D. Jones, International Journal of Climatology, 2005, **25**, 693-712.
33. T. Qian, A. Dai, K. E. Trenberth and K. W. Oleson, Journal of Hydrometeorology, 2006, **7**, 953-975.
34. G. C. Hurtt, S. Frolking, M. G. Fearon, B. Moore, E. Shevliakova, S. Malyshev, S. W. Pacala and R. A. Houghton, Global Change Biology, 2006, **12**, 1208-1229.
35. K. Klein Goldewijk, A. Beusen and P. Janssen, The Holocene, 2010, **20**, 565-573.
36. D. M. Lawrence, K. W. Oleson, M. G. Flanner, C. G. Fletcher, P. J. Lawrence, S. Levis, S. C. Swenson and G. B. Bonan, Journal of Climate, 2012, **25**, 2240-2260.
37. P. J. Lawrence and T. N. Chase, Journal of Geophysical Research: Biogeosciences, 2007, **112**, G01023.
38. M. C. Hansen, R. S. DeFries, J. R. G. Townshend, M. Carroll, C. Dimiceli and R. A. Sohlberg, Earth Interactions, 2003, **7**, 1-15.
39. A. Arneth, R. K. Monson, G. Schurgers, Ü. Niinemets and P. I. Palmer, Atmos. Chem. Phys., 2008, **8**, 4605-4620.
40. G. Schurgers, A. Arneth, R. Holzinger and A. H. Goldstein, Atmos. Chem. Phys., 2009, **9**, 3409-3423.
41. A. Guenther, T. Karl, P. Harley, C. Wiedinmyer, P. I. Palmer and C. Geron, Atmos. Chem. Phys., 2006, **6**, 3181-3210.
42. M. P. Chipperfield, Quarterly Journal of the Royal Meteorological Society, 2006, **132**, 1179-1203.
43. G. W. Mann, K. S. Carslaw, D. V. Spracklen, D. A. Ridley, P. T. Manktelow, M. P. Chipperfield, S. J. Pickering and C. E. Johnson, Geosci. Model Dev., 2010, **3**, 519-551.
44. D. V. Spracklen, K. J. Pringle, K. S. Carslaw, M. P. Chipperfield and G. W. Mann, Atmos. Chem. Phys., 2005, **5**, 2227-2252.
45. W. B. Rossow and R. A. Schiffer, B. Am. Meteorol. Soc., 1999, **80**, 2261-2287.

46. T. C. Bond, D. G. Streets, K. F. Yarber, S. M. Nelson, J.-H. Woo and Z. Klimont, J. Geophys. Res., 2004, **109**, D14203.
47. J. Cofala, M. Amann, Z. S. Klimont and W. Schopp, in Internal report of the Transboundary Air Pollution Programme, International Institute for Applied Systems Analysis, Laxenburg, Austria, 2005.
48. G. R. van der Werf, J. T. Randerson, L. Giglio, G. J. Collatz, M. Mu, P. S. Kasibhatla, D. C. Morton, R. S. DeFries, Y. Jin and T. T. van Leeuwen, Atmos. Chem. Phys., 2010, **10**, 11707-11735.
49. R. J. Andres and A. D. Kasgnoc, J. Geophys. Res., 1998, **103**, 25251-25261.
50. M. M. Halmer, H. U. Schmincke and H. F. Graf, Journal of Volcanology and Geothermal Research, 2002, **115**, 511-528.
51. N. A. Fuchs and A. G. Sutugin, in Topics in current aerosol research, eds. G. M. Hidy and J. R. Brock, Pergamin, New York, 1971, pp. 1-60.
52. C. E. Scott, D. V. Spracklen, J. R. Pierce, I. Riipinen, S. D. D'Andrea, A. Rap, K. S. Carslaw, P. M. Forster, P. Artaxo, M. Kulmala, L. V. Rizzo, E. Swietlicki, G. W. Mann and K. J. Pringle, Atmos. Chem. Phys., 2015, **15**, 12989-13001.
53. M. Kulmala, M. D. Maso, J. M. Mäkelä, L. Pirjola, M. Väkevä, P. Aalto, P. Miikkulainen, K. Hämeri and C. D. O'Dowd, Tellus B, 2001, **53**, 479-490.
54. S. A. Monks, S. R. Arnold, M. J. Hollaway, R. J. Pope, C. Wilson, W. Feng, K. M. Emmerson, B. J. Kerridge, B. L. Latter, G. M. Miles, R. Siddans and M. P. Chipperfield, Geosci. Model Dev. Discuss., 2016, **2016**, 1-51.
55. R. J. Pope, N. A. D. Richards, M. P. Chipperfield, D. P. Moore, S. A. Monks, S. R. Arnold, N. Glatthor, M. Kiefer, T. J. Breider, J. J. Harrison, J. J. Remedios, C. Warneke, J. M. Roberts, G. S. Diskin, L. G. Huey, A. Wisthaler, E. C. Apel, P. F. Bernath and W. Feng, Atmos. Chem. Phys., 2016, **16**, 13541-13559.
56. U. Pöschl, R. von Kuhlmann, N. Poisson and P. J. Crutzen, Journal of Atmospheric Chemistry, 2000, **37**, 29-52.
57. D. E. Kinnison, G. P. Brasseur, S. Walters, R. R. Garcia, D. R. Marsh, F. Sassi, V. L. Harvey, C. E. Randall, L. Emmons, J. F. Lamarque, P. Hess, J. J. Orlando, X. X. Tie, W. Randel, L. L. Pan, A. Gettelman, C. Granier, T. Diehl, U. Niemeier and A. J. Simmons, Journal of Geophysical Research: Atmospheres, 2007, **112**, n/a-n/a.
58. L. K. Emmons, S. Walters, P. G. Hess, J. F. Lamarque, G. G. Pfister, D. Fillmore, C. Granier, A. Guenther, D. Kinnison, T. Laepple, J. Orlando, X. Tie, G. Tyndall, C. Wiedinmyer, S. L. Baughcum and S. Kloster, Geosci. Model Dev., 2010, **3**, 43-67.
59. L. K. Emmons, S. R. Arnold, S. A. Monks, V. Huijnen, S. Tilmes, K. S. Law, J. L. Thomas, J. C. Raut, I. Bouarar, S. Turquety, Y. Long, B. Duncan, S. Steenrod, S. Strode, J. Flemming, J. Mao, J. Langner, A. M. Thompson, D. Tarasick, E. C. Apel, D. R. Blake, R. C. Cohen, J. Dibb, G. S. Diskin, A. Fried, S. R. Hall, L. G. Huey, A. J. Weinheimer, A. Wisthaler, T. Mikoviny, J. Nowak, J. Peischl, J. M. Roberts, T. Ryerson, C. Warneke and D. Helmig, Atmos. Chem. Phys., 2015, **15**, 6721-6744.
60. Q. Zhang, D. G. Streets, G. R. Carmichael, K. B. He, H. Huo, A. Kannari, Z. Klimont, I. S. Park, S. Reddy, J. S. Fu, D. Chen, L. Duan, Y. Lei, L. T. Wang and Z. L. Yao, Atmos. Chem. Phys., 2009, **9**, 5131-5153.
61. C. Granier, J. Lamarque, A. Mieville, J. Muller, J. Olivier, J. Orlando, J. Peters, G. Petron, G. Tyndall and S. Wallens, POET, http://accent.aero.jussieu.fr/database_table_inventories.php).
62. J. G. J. Olivier and J. J. M. Berdowski, in The Climate System, eds. J. Berdowski, R. Guicherit and B. J. Heij, A.A. Balkema Publishers/Swets & Zeitlinger Publishers, Lisse, The Netherlands, 2001, pp. 33-78.
63. A. A. Bloom, P. I. Palmer, A. Fraser and D. S. Reay, Biogeosciences, 2012, **9**, 2821-2830.
64. P. K. Patra, S. Houweling, M. Krol, P. Bousquet, D. Belikov, D. Bergmann, H. Bian, P. Cameron-Smith, M. P. Chipperfield, K. Corbin, A. Fortems-Cheiney, A. Fraser, E. Gloor, P. Hess, A. Ito, S. R. Kawa, R. M. Law, Z. Loh, S. Maksyutov, L. Meng, P. I. Palmer, R. G. Prinn, M. Rigby, R. Saito and C. Wilson, Atmos. Chem. Phys., 2011, **11**, 12813-12837.
65. C. Wilson, M. Gloor, L. V. Gatti, J. B. Miller, S. A. Monks, J. McNorton, A. A. Bloom, L. S. Basso and M. P. Chipperfield, Global Biogeochemical Cycles, 2016, **30**, 400-420.
66. L. Zhang, S. Gong, J. Padro and L. Barrie, Atmospheric Environment, 2001, **35**, 549-560.
67. J. M. Edwards and A. Slingo, Quarterly Journal of the Royal Meteorological Society, 1996, **122**, 689-719.
68. N. Bellouin, G. W. Mann, M. T. Woodhouse, C. Johnson, K. S. Carslaw and M. Dalvi, Atmos. Chem. Phys., 2013, **13**, 3027-3044.

69. D. V. Spracklen, K. S. Carslaw, U. Pöschl, A. Rap and P. M. Forster, Atmos. Chem. Phys., 2011, **11**, 9067-9087.
70. A. Nenes and J. H. Seinfeld, J. Geophys. Res., 2003, **108**, 4415.
71. C. Fountoukis and A. Nenes, J. Geophys. Res., 2005, **110**, D11212.
72. D. Barahona, R. E. L. West, P. Stier, S. Romakkaniemi, H. Kokkola and A. Nenes, Atmos. Chem. Phys., 2010, **10**, 2467-2473.
73. M. D. Petters and S. M. Kreidenweis, Atmos. Chem. Phys., 2007, **7**, 1961-1971.
74. G. J. Engelhart, A. Asa-Awuku, A. Nenes and S. N. Pandis, Atmos. Chem. Phys., 2008, **8**, 3937-3949.
75. G. J. Engelhart, R. H. Moore, A. Nenes and S. N. Pandis, J. Geophys. Res., 2011, **116**, D02207.
76. U. Dusek, G. P. Frank, J. Curtius, F. Drewnick, J. Schneider, A. Kürten, D. Rose, M. O. Andreae, S. Borrmann and U. Pöschl, Geophys. Res. Lett., 2010, **37**, L03804.
77. S. S. Gunthe, S. M. King, D. Rose, Q. Chen, P. Roldin, D. K. Farmer, J. L. Jimenez, P. Artaxo, M. O. Andreae, S. T. Martin and U. Pöschl, Atmos. Chem. Phys., 2009, **9**, 7551-7575.
78. A. Rap, N. A. D. Richards, P. M. Forster, S. A. Monks, S. R. Arnold and M. P. Chipperfield, Geophysical Research Letters, 2015, **42**, 5074-5081.
79. V. Naik, D. Mauzerall, L. Horowitz, M. D. Schwarzkopf, V. Ramaswamy and M. Oppenheimer, Journal of Geophysical Research: Atmospheres, 2005, **110**, n/a-n/a.
80. P. Forster, V. Ramaswamy, P. Artaxo, T. Berntsen, R. Betts, D. W. Fahey, J. Haywood, J. Lean, D. C. Lowe, G. Myhre, J. Nganga, R. Prinn, G. Raga, M. Schulz and R. V. Dorland, in Climate Change 2007: The Physical Science Basis. Contribution of Working Group I to the Fourth Assessment Report of the Intergovernmental Panel on Climate Change, eds. S. Solomon, D. Qin, M. Manning, Z. Chen, M. Marquis, K. B. Averyt, M.Tignor and H. L. Miller, Cambridge University Press, Cambridge, UK and New York, USA, 2007, ch. 2.
81. M. G. Lawrence, P. Jöckel and R. von Kuhlmann, Atmos. Chem. Phys., 2001, **1**, 37-49.
82. J. S. Fuglestvedt, T. K. Berntsen, I. S. A. Isaksen, H. Mao, X.-Z. Liang and W.-C. Wang, Atmospheric Environment, 1999, **33**, 961-977.
83. T. K. Berntsen, J. S. Fuglestvedt, M. M. Joshi, K. P. Shine, N. Stuber, M. Ponater, R. Sausen, D. A. Hauglustaine and L. Li, Tellus B, 2005, **57**, 283-304.
84. C. D. Holmes, M. J. Prather, O. A. Søvde and G. Myhre, Atmos. Chem. Phys., 2013, **13**, 285-302.
85. G. Myhre, E. J. Highwood, K. P. Shine and F. Stordal, Geophys. Res. Lett., 1998, **25**.
86. G. Myhre, D. Shindell, F.-M. Bréon, W. Collins, J. Fuglestvedt, J. Huang, D. Koch, J.-F. Lamarque, D. Lee, B. Mendoza, T. Nakajima, A. Robock, G. Stephens, T. Takemura and H. Zhan, in Climate Change 2013: The Physical Science Basis. Contribution of Working Group I to the Fifth Assessment Report of the Intergovernmental Panel on Climate Change, eds. T. F. Stocker, D. Qin, G.-K. Plattner, M. Tignor, S. K. Allen, J. Boschung, A. Nauels, Y. Xia, V. Bex and P. M. Midgley, Cambridge University Press, Cambridge, United Kingdom and New York, NY, USA, 2013, ch. 8.
87. A. H. Goldstein and I. E. Galbally, Environmental Science & Technology, 2007, **41**, 1514-1521.
88. R. J. Griffin, D. R. Cocker, III, J. H. Seinfeld and D. Dabdub, Geophys. Res. Lett., 1999, **26**, 2721-2724.
89. M. Kanakidou, J. H. Seinfeld, S. N. Pandis, I. Barnes, F. J. Dentener, M. C. Facchini, R. Van Dingenen, B. Ervens, A. Nenes, C. J. Nielsen, E. Swietlicki, J. P. Putaud, Y. Balkanski, S. Fuzzi, J. Horth, G. K. Moortgat, R. Winterhalter, C. E. L. Myhre, K. Tsigaridis, E. Vignati, E. G. Stephanou and J. Wilson, Atmos. Chem. Phys., 2005, **5**, 1053-1123.
90. C. L. Heald, D. A. Ridley, S. M. Kreidenweis and E. E. Drury, Geophysical Research Letters, 2010, **37**, L24808.
91. C. L. Heald, H. Coe, J. L. Jimenez, R. J. Weber, R. Bahreini, A. M. Middlebrook, L. M. Russell, M. Jolleys, T. M. Fu, J. D. Allan, K. N. Bower, G. Capes, J. Crosier, W. T. Morgan, N. H. Robinson, P. I. Williams, M. J. Cubison, P. F. DeCarlo and E. J. Dunlea, Atmos. Chem. Phys., 2011, **11**, 12673-12696.
92. D. V. Spracklen, J. L. Jimenez, K. S. Carslaw, D. R. Worsnop, M. J. Evans, G. W. Mann, Q. Zhang, M. R. Canagaratna, J. Allan, H. Coe, G. McFiggans, A. Rap and P. Forster, Atmos. Chem. Phys., 2011, **11**, 12109-12136.
93. K. Tsigaridis, N. Daskalakis, M. Kanakidou, P. J. Adams, P. Artaxo, R. Bahadur, Y. Balkanski, S. E. Bauer, N. Bellouin, A. Benedetti, T. Bergman, T. K. Berntsen, J. P. Beukes, H. Bian, K. S. Carslaw, M. Chin, G. Curci, T. Diehl, R. C. Easter, S. J. Ghan, S. L. Gong, A. Hodzic, C. R. Hoyle, T. Iversen, S. Jathar, J. L. Jimenez, J. W. Kaiser, A. Kirkevåg, D. Koch, H. Kokkola, Y. H. Lee, G. Lin, X. Liu, G. Luo, X. Ma, G. W. Mann, N. Mihalopoulos, J. J. Morcrette, J. F. Müller, G. Myhre, S. Myriokefalitakis, N. L. Ng, D. O'Donnell, J. E. Penner, L. Pozzoli, K. J. Pringle, L. M. Russell, M. Schulz, J. Sciare, Ø. Seland,

D. T. Shindell, S. Sillman, R. B. Skeie, D. Spracklen, T. Stavrakou, S. D. Steenrod, T. Takemura, P. Tiitta, S. Tilmes, H. Tost, T. van Noije, P. G. van Zyl, K. von Salzen, F. Yu, Z. Wang, Z. Wang, R. A. Zaveri, H. Zhang, K. Zhang, Q. Zhang and X. Zhang, Atmos. Chem. Phys., 2014, **14**, 10845-10895.

94. A. Voulgarakis, V. Naik, J. F. Lamarque, D. T. Shindell, P. J. Young, M. J. Prather, O. Wild, R. D. Field, D. Bergmann, P. Cameron-Smith, I. Cionni, W. J. Collins, S. B. Dalsøren, R. M. Doherty, V. Eyring, G. Faluvegi, G. A. Folberth, L. W. Horowitz, B. Josse, I. A. MacKenzie, T. Nagashima, D. A. Plummer, M. Righi, S. T. Rumbold, D. S. Stevenson, S. A. Strode, K. Sudo, S. Szopa and G. Zeng, Atmos. Chem. Phys., 2013, **13**, 2563-2587.

95. D. Taraborrelli, M. G. Lawrence, J. N. Crowley, T. J. Dillon, S. Gromov, C. B. M. Grosz, L. Vereecken and J. Lelieveld, Nature Geosci, 2012, **5**, 190-193.

96. H. Fuchs, A. Hofzumahaus, F. Rohrer, B. Bohn, T. Brauers, H. P. Dorn, R. Haseler, F. Holland, M. Kaminski, X. Li, K. Lu, S. Nehr, R. Tillmann, R. Wegener and A. Wahner, Nature Geosci, 2013, **6**, 1023-1026.

97. D. S. Ward and N. M. Mahowald, Earth Syst. Dynam., 2015, **6**, 175-194.

98. H. Hakola, H. Hellén, M. Hemmilä, J. Rinne and M. Kulmala, Atmos. Chem. Phys., 2012, **12**, 11665-11678.

99. K. Jardine, A. Yañez Serrano, A. Arneth, L. Abrell, A. Jardine, J. van Haren, P. Artaxo, L. V. Rizzo, F. Y. Ishida, T. Karl, J. Kesselmeier, S. Saleska and T. Huxman, J. Geophys. Res., 2011, **116**, D19301.

100. C. R. Hoyle, M. Boy, N. M. Donahue, J. L. Fry, M. Glasius, A. Guenther, A. G. Hallar, K. Huff Hartz, M. D. Petters, T. Petäjä, T. Rosenoern and A. P. Sullivan, Atmos. Chem. Phys., 2011, **11**, 321-343.

101. M. Hallquist, J. C. Wenger, U. Baltensperger, Y. Rudich, D. Simpson, M. Claeys, J. Dommen, N. M. Donahue, C. George, A. H. Goldstein, J. F. Hamilton, H. Herrmann, T. Hoffmann, Y. Iinuma, M. Jang, M. E. Jenkin, J. L. Jimenez, A. Kiendler-Scharr, W. Maenhaut, G. McFiggans, T. F. Mentel, A. Monod, A. S. H. PrÃ©vÃ´t, J. H. Seinfeld, J. D. Surratt, R. Szmigielski and J. Wildt, Atmos. Chem. Phys., 2009, **9**, 5155-5236.

102. H. Gordon, K. Sengupta, A. Rap, J. Duplissy, C. Frege, C. Williamson, M. Heinritzi, M. Simon, C. Yan, J. Almeida, J. Tröstl, T. Nieminen, I. K. Ortega, R. Wagner, E. M. Dunne, A. Adamov, A. Amorim, A.-K. Bernhammer, F. Bianchi, M. Breitenlechner, S. Brilke, X. Chen, J. S. Craven, A. Dias, S. Ehrhart, L. Fischer, R. C. Flagan, A. Franchin, C. Fuchs, R. Guida, J. Hakala, C. R. Hoyle, T. Jokinen, H. Junninen, J. Kangasluoma, J. Kim, J. Kirkby, M. Krapf, A. Kürten, A. Laaksonen, K. Lehtipalo, V. Makhmutov, S. Mathot, U. Molteni, S. A. Monks, A. Onnela, O. Peräkylä, F. Piel, T. Petäjä, A. P. Praplan, K. J. Pringle, N. A. D. Richards, M. P. Rissanen, L. Rondo, N. Sarnela, S. Schobesberger, C. E. Scott, J. H. Seinfeld, S. Sharma, M. Sipilä, G. Steiner, Y. Stozhkov, F. Stratmann, A. Tomé, A. Virtanen, A. L. Vogel, A. C. Wagner, P. E. Wagner, E. Weingartner, D. Wimmer, P. M. Winkler, P. Ye, X. Zhang, A. Hansel, J. Dommen, N. M. Donahue, D. R. Worsnop, U. Baltensperger, M. Kulmala, J. Curtius and K. S. Carslaw, Proceedings of the National Academy of Sciences, 2016, **113**, 12053-12058.

Acknowledgements

We acknowledge support from EU Horizon 2020 (SC5-01-2014; grant agreement no 641816), NERC (NE/H524673/1, NE/J004723/1, NE/G015015/1, NE/K015966/1), EPSRC (EP/I014721/1) and the United Bank of Carbon (UBoC). This work used ARC, part of the High Performance Computing Facilities at the University of Leeds, UK.

Author Contributions

C.E.S. and D.V.S. designed the experiments. C.E.S. and S.A.M. performed the model simulations. A. R., M. P. C., C.L.R., and C.W. provided data for model simulations and subsequent calculations. C.E.S. performed the analysis. All authors contributed to scientific discussion and helped write the manuscript.

Competing Interests

The authors declare no competing financial interests.